Automatic Detection of In-field Defect Growth in Image Sensors

Jenny Leung, Glenn H. Chapman

School of Engineering Science
Simon Fraser University
Burnaby, B.C., Canada, V5A 1S6
jla98@sfu.ca, glennc@ensc.sfu.ca

Israel Koren, Zahava Koren

Dept. of Electrical and Computer Engineering
University of Massachusetts
Amherst, MA, 01003
koren,zkoren@ecs.umass.edu

Abstract

Characterization of in-field defect growth with time in digital image sensors is important for measuring the quality of sensors as they age. While more defects were found in cameras exposed to high cosmic ray radiation environments, comparing the collective growth rate of different sensor types has shown that CCD imagers develop twice as many defects as APS imagers, indicating that CCD imagers may be more sensitive to radiation. The defect growth of individual imagers can be estimated by analyzing historical image sets captured by individual cameras. This paper presents a defect tracing algorithm, which determines the presence or absence of defects by accumulating Bayesian statistics collected over a sequence of images. Recognizing the complexity of image scenes, camera settings, and local clustering of defects in color images (due to demosaicing), refinements of the algorithm have been explored and the resulting detection accuracy has increased significantly. In-field test results from 3 imagers with a total of 26 defects have shown that 96% of the defects' dates were identified with less than 10 days difference compared to visual inspection. In addition to our continuous study of in-field defects in high-end digital SLRs, this paper presents a preliminary study of 10 cellphone cameras. Our test results address the comparison of defects types, distribution and growth found in low-end and high-end cameras with significantly different pixel sizes.

1. Introduction

Over the last decade, digital imagers have become increasingly popular in many products. Unfortunately, like all microelectronic devices, digital imagers are prone to develop defects over their lifetime. Furthermore, unlike digital circuits, imager pixels are analog devices, so defects that would not affect digital devices will manifest themselves in these pixels. Advancements in image processing techniques have significantly improved the quality of digital images; however, very little has been done to address in-field defects in digital imagers. Moreover, ignoring the presence of defects during the processing of images causes faulty pixels to smear into neighboring pixels and significantly degrade the image quality. Our previous study has shown that defects in digital imagers are permanent and increase in number continuously over time and consequently, such defects will manifest themselves in all captured images [1]. Although defects can be hidden by sending the camera back for factory calibration, this is in most cases very expensive and time consuming or simply impossible. Thus, with the integration of image sensors in many portable devices, exploration of in-field defect correction techniques is needed.

In our on-going study [1], we have characterized in-field defects by analyzing their spatial distribution, and tracing the growth of defects in a set of semi-professional cameras. Our study has shown that defects are not likely related to material degradation. In fact, the initial analysis of

1550-5774/08 $25.00 © 2008 IEEE
DOI 10.1109/DFT.2008.58

results in another study [2], had suggested that the defect rate would be higher for sensors that have been through more transatlantic/pacific flights, which we have also seen in our tested cameras. However, to verify the driving force of high defect rates during long high-altitude air flights, we must collect defect data from a wider range of cameras. Our recent work [3] has focused on developing a set of software tools that allow us to collect in-field defect samples from a wider set of imagers. In particular, we have proposed a defect-tracing algorithm that can identify the first appearance of defects through analysis of a sequence of images. The development of this algorithm has not only allowed us to better observe the quality of an aging image sensor; it can potentially become an embedded solution to correct any identified defects as they develop. In this paper, we extend this work by applying the algorithm to image data sets from our tested cameras as well as explore possible enhancement to improve the accuracy of the detection. To further extend our study of high-end DSLRs, we started experiments on cellphone cameras, which have smaller pixels and different characteristics compared to DSLRs.

2. Defects Characteristics

Expanding our on-going study [4] we are currently identifying in-field defects from 12 semi-professional cameras that include sensor technologies from both Charge Couple Device (CCD) and Active Pixel Sensors (APS). While our previous study had concluded that defects only impact single isolated pixels, in any pictures, a faulty pixel will appear as a cluster in color images due to their spreading during internal image processing steps such as noise reduction, color interpolation (demosaicing), and image compressing. Defect clusters are more noticeable than a single faulty pixel; therefore, defects in image sensors are highly undesirable. Thus, a detailed study of in-field defects can provide us with better understanding of the defect source mechanism.

2.1 Defect Identification

Our recent laboratory calibration result on 12 cameras in Table 1 again shows that hot pixels are the dominant type of defects in all tested cameras. In-field defects are identified by performing a dark-frame calibration where a set of images is captured in the absence of light with increasing exposure settings. With the new imagers added to our collection of cameras and additional defects appearing in the other cameras, our defect number had increased from 98 [1] to 136 allowing us to increase the statistical relevance of our defect analysis.

Based on our laboratory calibration, we have identified two types of hot pixels: standard hot pixel and partial stuck hot pixel. The dark-frame response of the hot pixels is shown in Figure 1. A standard hot pixel is characterized by an illumination independent component that increases with exposure time, as shown in curve (a). On the other hand, a partially stuck hot pixel has an additional offset that can be observed even in the absence of light, as shown in curve (b). The presence of a dark current will reduce the dynamic range of the pixel in addition to the offset. The phenomenon of these two types of hot pixels can be summarized by

$$f_{Hot-Pixel}(I_{photo}, I_{Dark}, T_{Integration}) = m \cdot (I_{photo} T_{Integration} + I_{Dark} T_{Integration}) + b\,, \qquad (1)$$

I_{photo} is the incident illumination on the pixel, $T_{intergration}$ is the exposure duration, I_{dark} is a unique dark current at each pixel site, and *b* is the additional offset found in partially stuck hot pixels.

Table 1. Summary of identified hot pixels from all tested cameras.

Camera	Number of defects found			
	Hot			**Total**
	No offset	W/ offset	*Total*	
A	0	11	11	11
B	17	0	17	17
C	6	5	11	11
D	0	0	0	0
E	26	0	26	26
F	0	5	5	5
G	0	2	2	2
H	3	0	3	3
I	2	17	19	19
J	4	27	31	31
K	9	1	10	10
L	0	2	2	2
			Cumulative total	**137**

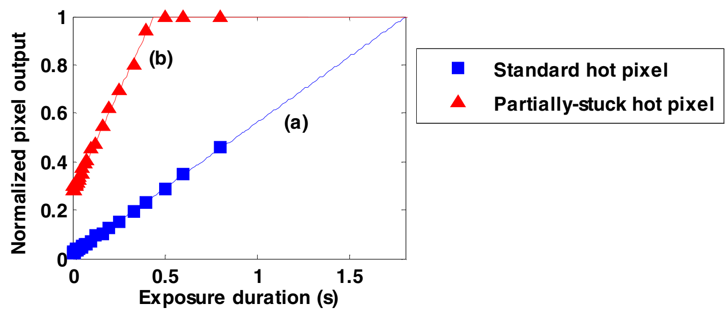

Figure 1. Dark Response of (a) standard hot pixel and (b) partially stuck hot pixel

2.2 Temporal and spatial growth of defects

In our previous study [1] we have shown that defects develop continuously throughout the sensor lifetime and these in-field defects are irrevocable. To better understand the defect source mechanism we have analyzed the spatial distribution of defects using the most recent collection of defects as shown in Figure 2a, see [1] for the analysis procedure. When there is local clustering of defects we should have observed multiple local peaks around long and short distances. However, with a broad distance distribution and an average distance of about 10mm, there is clearly no indication of defect clusters. While the minimum distance of 17μm between faulty pixels, where pixels size is ~(6-7 μm), this result is again consistent with our claim that defects are caused by a random process and not by material degradation. The most likely cause is cosmic ray induced defect damage which is a purely time random process [1].

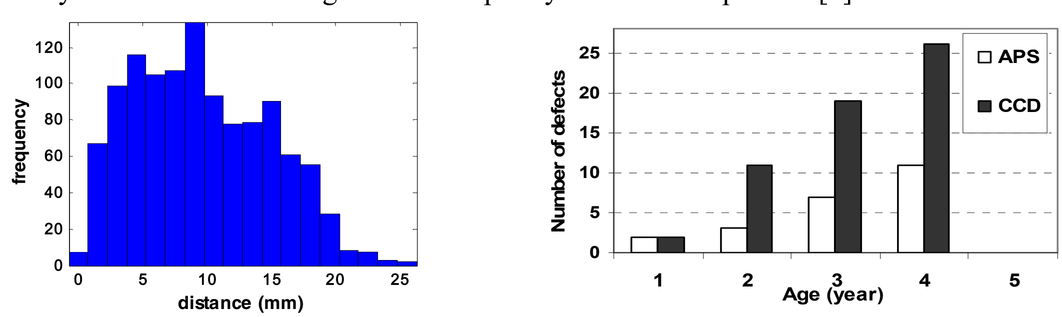

(a) Spatial distribution of defects **(b) Temporal growth of defects**

Figure 2. Defects growth for APS and CCD cameras.

In Figure 2b we compare the number of defects collected from the 5 APS and 7 CCD cameras, using the average number of defects collected at various ages of each sensor type. As this plot indicates, the development of defects is a continuous process in both sensors; however, there is a significant difference in the defect growth rate between the two types of sensors. The average defect growth rate of APS imagers is ~2.2 defects/year while for CCD imagers it is ~5.2 defects/year; thus we are seeing twice more defects in CCD than in APS imagers at the same age, yet both detectors have approximately the same image area and pixel area. We observed high defect numbers in cameras that have been through high altitude and long flights due to the ~100 times higher radiation levels during those flights [2]. However, this is more noticeable in CCD imagers, where we observed as many as 20 defects within one year from a camera that has been on four international flights. For this reason imagers with many air flights were not considered in this growth analysis so it not skewed by the external conditions. Although there is no clear explanation to the different defect rate, our preliminary results suggest that CCD may be more sensitive to cosmic ray radiation.

The temporal growth rate of defects in individual sensors can be obtained by analyzing the full historical image collection from these imagers. Defects within pictures can often be identified by visual inspection; however, this manual technique is time consuming and due to privacy concerns we cannot gain access to a wider range of datasets. In our most recent study [3] we had proposed a defect-tracing algorithm that can automatically detect the first appearance of a defect by analyzing a sequence of color images. Simulation experiments have shown the effectiveness of this algorithm. In this paper we extend this algorithm and use it to experimentally determine the time development of defects from our set of tested cameras. We determine the accuracy of the detection algorithm based on comparison with the detect dates found from visual inspection. Once this algorithm is proven to operate with sufficient accuracy, we can provide end-users with a software tool that will collect defect growth data by analyzing their image dataset.

3. Defect tracing algorithm

Automatic defect tracing from color images enables a more quantitative analysis of how in-field defects develop over the lifetime of digital imagers. More importantly, with the ability to detect the appearance of defects, we can develop an in-field scheme for the correction of in-field defects. As described in Section 2, hot pixels are the dominant defects found in all tested cameras, thus the main interest of our tracing algorithm is to estimate the first appearance date of these hot pixels by analyzing the image datasets from individual imagers.

Most camera users capture images in RGB color mode, where each color is composed of red, green and blue (RGB) values. One main challenge in detecting defects in color images is the irreversible post-processing algorithm applied to the captured images prior to the observed output. In any digital camera, the initial image captured is called a raw image where each pixel will only record one of the three color channels (red, green or blue) as shown in Figure 3. To produce a color image, demosaicing, an internal color interpolation algorithm is used to interpolate the two missing color channels at each pixel site. As one can expect, if a pixel is defective, interpolating with the inaccurate response of the pixel will spread the error to neighboring pixels; thus we will observe a cluster of defective pixels in color images as shown in Figure 4 [3]. While digital raw photos permit us to extract the pixels before this spread, most photos are not saved in that format.

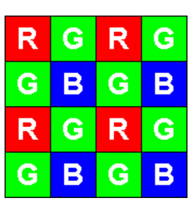

Figure 3. Raw image pattern.

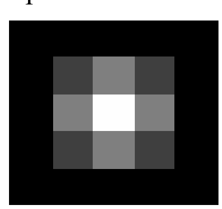

Figure 4. Demosaic image output with defect

3.1 Pixel value estimation

In order to estimate the first defective date for any faulty pixel, our algorithm needs to detect the presence or absence of the known hot pixels, obtained from simple calibration tests with digital raw images at the identified locations. In our algorithm, each sensor is represented by an array of $W \times H$ pixels, and we denote the output of each pixel by $y_{i,j}$ where (i,j) is the location of the pixel. To properly identify defects in images, we model the behavior of each pixel with Equation (1), where I_{dark} is zero for a good pixel, and the locations and unique dark current values of each hot pixel are mapped out using a dark frame calibration.

The expected value of a pixel, denoted by $z_{i,j}$, can be estimated by interpolation with neighboring pixels. Given a good interpolation scheme, the interpolation error $e_{i,j} = y_{i,j} - z_{i,j}$, of a good pixel is approximately zero; however, in the case of a hot pixel, the dark current and the additional offset will result in a larger interpolation error. By collecting the image-wide interpolation error we can derive the interpolation error Probability Density Function (PDF), $p_E(e)$ the probability of a good pixel given its value y_k and the interpolation z_k, and the Cumulative Density Function (CDF), $P_E(e)$, which provide a statistical measure of the state of the defective pixel, are given in Equations (2) and (3) (see [3] for the detailed derivation of these equations)..

$$Prob(y_k \mid Good) = p_E(y_k - z_k) \tag{2}$$

$$Prob(y \mid Hot) = \frac{1}{255 - \Delta_{\min} + 1} \cdot \left[P_E(y - z - \Delta_{\min}) - P_E(y - z - 255) \right] \tag{3}$$

Because most picture sets only have access to jpg pictures which contain the demosaic spread defects we need to compensated for that in our search. The key to estimating the presence of a faulty pixel is related to the accuracy of the interpolation scheme from the neighboring pixels. With a simple 3×3 averaging, we would expect to have sufficient accuracy; however, as indicated by Figure 4, due to the application of the demosaicing process to color images, the nearest neighbors are the most distorted by the defects. Because single defects appear as local clusters in color images, the expected output of a defective pixel would be more accurate if we employ a larger interpolation region that are further away, such as 5×5 and 7×7 and eliminate the nearest neighbor region (because those will be affected by the defect presence) with a ring averaging mask shown in Figure 5. With the ring averaging, we can estimate pixel output and avoid the problem of the local defect cluster.

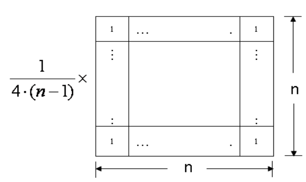

Figure 5. Ring averaging coefficient mask.

3.2 Bayesian accumulation detection

Pixel estimation can provide a measure of the likelihood of a pixel being good or defective at one single image. However, the decision on the status of a pixel cannot rely solely on analysis of one image. External factors such as the complexity of an image scene, the capturing mode such as ISO, and the exposure setting will affect the visibility of defects in different images. To accumulate statistics over a sequence of images, we use Bayesian statistics as shown in Equations (4) and (5) which evaluate the likelihood of having a good/hot pixel at the k-th image.

$$Prob(Good \mid y_k) = \frac{Prob(y_k \mid Good) \cdot Prob(Good \mid y_{k-1})}{Prob(y_k \mid Good) \cdot Prob(Good \mid y_{k-1}) + Prob(y_k \mid Hot) \cdot Prob(Hot \mid y_{k-1})} \tag{4}$$

$$Prob(Hot \mid y_k) = 1 - Prob(Good \mid y_k). \quad (5)$$

By accumulating statistics on the status of pixels using Equation (4), detection of a good pixel is indicated by $Prob(Good|y_k)$ ~1, and when $Prob(Good|y_k)$ is ~0, this will indicate that the pixel has become defective as shown in Figure 6. However, when a large number of images is accumulated, saturation of the accumulated probability may become a problem. In addition, because most regular images are captured in short exposure range, hot pixels with low dark current magnitude are not easily observed, and the change in the accumulated probability will not be reflected. Thus, to better detect the instantaneous change of the pixel status, a sliding window approach is used as shown in Figure 7. The sliding window approach will determine the status of the pixel by accumulating statistics from the *n* most recently analyzed images. Previous simulation results [3] have shown that a window length of 5 or 7 tends to attenuate the detection date whereas with a length of 3, more emphasis is put on the recent images and older imagers are ignored. Thus we will focus on using a window length of 3 only.

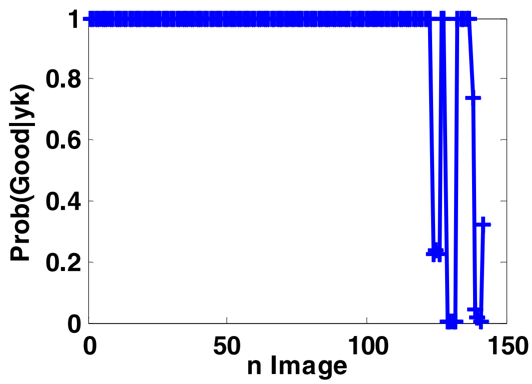

Figure 6. Probability accumulated over sequence of images

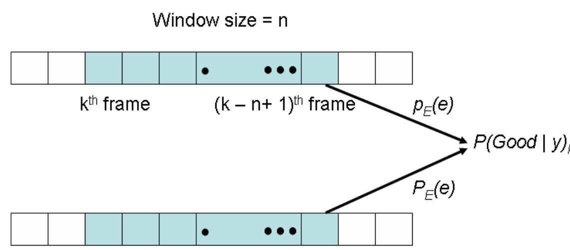

Figure 7. Sliding window

3.3 Local region analysis

Analyzing pictures is a complicated procedure; external factors such as the complexity of image scenes, ISO settings, exposure setting, and dark current magnitude will all affect the performance of our detection procedure. Local regions with edge or fine details tend to have more color variation, thus large estimation errors are unavoidable. Images taken at high ISO setting are grainier; therefore, a region with similar colors can still result in large variations. To improve the accuracy of the algorithm, these external factors must be taken into consideration. Because fine details are usually localized in a region; ignoring images with lots of details will potentially flush away other useful information. Instead of discarding images, we applied a post-procedure where we attempted to correct the detected defect date by incorporating some knowledge of local region around the defect. The complexity of any local region can be measured by evaluating the mean and variance of each color channel separately. Given these two measurements, we can simply set a threshold on these parameters and correct detection caused by inaccurate estimation of a pixel output. In our experiments, we performed detection with and without local statistics and analyzed the trade-off with the additional correction procedure.

4. Automated defect growth detection

Using the developed software, we accessed the historical images of three of our test cameras. The three cameras are 2 to 5 years old, with resolution varying from 6M to 10M and a total of 26 hot pixels. The development dates of defects were detected both by the automatic defect-tracing algorithm and by visual inspection. To evaluate the performance of our detection algorithm, we calculate the detection error that is the difference between the algorithm-detected defect date and the observed defect date. Due to the spreading of defects we have experimented with 3×3, 5×5 and 7×7 ring averaging. In addition, to better examine the improvement of the local analysis correction, we compared the detected dates with and without local analysis correction. Figure 6 summarizes our results by plotting the frequencies of the detection errors.

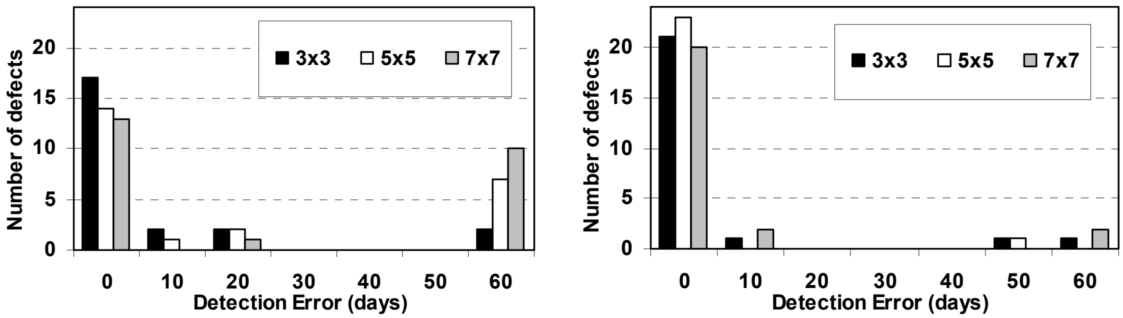

(a) Without local correction **(b) With local correction**

Figure 8. Detection error (a) without local correction, (b) with local correction.

As shown in Figure 8a, the detection error results without correction with a 3×3 averaging achieved the highest accuracy among the three interpolation schemes where 71% of the defects were identified within 10 days of the observed date. But errors of up to 60 days were found. With 5×5 and 7×7 ring averaging we observed significantly more outliers with error >60 days. The majority of detection errors are caused by false identification of defects when the faulty pixel is located in a fine detailed color region. Thus, to correct these errors, a localized analysis around the defective region can help determine if the detection is simply an interpolation error or the first appearance of a defect. By recognizing details from the local region analysis, false detection can be corrected and the results in Figure 8b show a significant improvement in the accuracy of the detection. In fact, the 5×5 ring averaging now achieves the highest accuracy with 96% of defects identified with less than 10 days error. Although the accuracy with 3×3 averaging had increased to 88%; it is clear that this averaging scheme still has some large outliers of 50 – 60 days. As discussed in Section 3, the spreading of defects caused by the demosaicing algorithm is most significant in the nearest neighbors, thus 3×3 averaging cannot provide a good approximation to the expected pixel value. Defects can become undetectable when the neighboring pixels are highly distorted by the defects, thus these outliers simply indicate the limitation of the 3×3 interpolation scheme. On the other hand, with 7×7 ring averaging, 83% of defects were detected with error <10 days. However, the large interpolation region required by this averaging scheme induces more estimation errors; thus this interpolation does not provide a very robust detection result. In all cases it must be remembered that the detection error is highly dependent on the dates on which the images were taken. Because most camera users do not capture images at a steady rate, inherently, part of the detection error can be caused by large gaps between two sequential image. This error is simply inevitable where when the detection is difference by one image can be interpreted as anything from one day to 50 days as some picture data bases show.

Knowing the defect development date of each defect, we can estimate the defect growth rate for all three tested cameras. Figure 9 shows a comparison of the defect growth rates based on visual inspection and on the detection algorithm with the 5×5 interpolation scheme. In particular, a linear fit function is used to estimate the defect growth rate for each test camera.

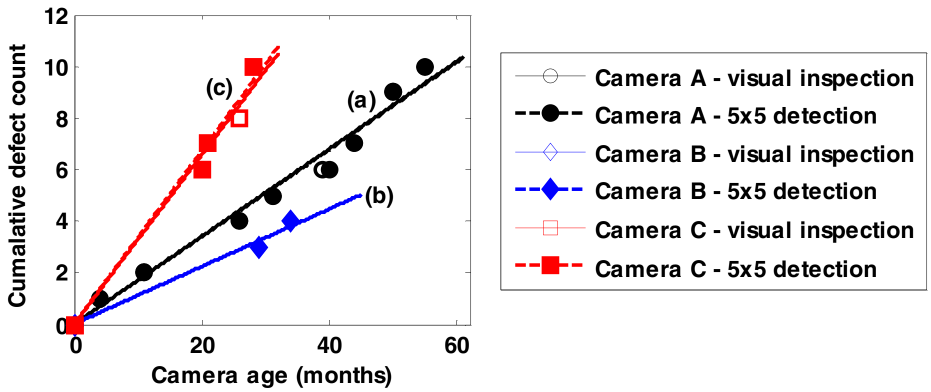

Figure 9. Temporal defect growth of (a) camera A, (b) camera B, (c) camera C.

The observed and detected defect growth rates (found by the detection algorithm) with different interpolation schemes are summarized in Table 2. Again, by comparing the detect growth rate to that estimated from visual inspection, the results with 5×5 averaging achieve the best approximation of the growth rate where camera A, and Bare both APS imagers and camera C is a CCD imager.

Table 2. Defect growth rate results from detection algorithm with local correction.

	Observed defect growth rate (defects / year)	**Detected defect growth rate (defects / year)**		
		3x3 Averaging	5x5 Averaging	7x7 Averaging
Camera A	2.04	1.99	2.03	2.08
Camera B	1.34	1.32	1.34	1.34
Camera C	3.94	4.04	4.04	3.74

5. Defects characterization in cellphone cameras

The popularity of integrated image sensors in devices such as cellphone has increased over the past few years. To extend our analysis, we expanded our data collection to include a set of high-end cellphone cameras. In this study we collect in-field defects from a set of 10 mobile phone cameras of the same model. Cellphone cameras do not have the advanced capability of capturing raw images, have no explicit control on exposure setting, and standard laboratory dark calibration cannot be performed on these cameras. To estimate the number of defects in these cameras, we performed dark frame calibration by capturing dark images in color mode, and the results are summarized in Table 3.

Table 3. Summary of identified defects cellphone cameras.

	Hot pixels		
Camera	No offset	w/offset	**Total**
A	6	3	9
B	11	2	13
C	6	2	8
D	4	2	6
E	6	6	12
F	12	2	14
G	10	4	14
H	6	4	10
I	9	5	14
J	7	10	17
		Cumulative total	117

With shrinkage in the pixel dimensions to 2.2 μm, defect clusters in these sensors are more likely to occur and the impact of hot pixels can be more significant. Moreover these cameras only have 5.7x4.3 mm sensors, only 7% the size of the 24x15 mm DSLR sensors. Because internal processing algorithms such as demosaicing and image compression will distort the defects in color images, we cannot at this point conclude if defects in these sensors are cluster-free nor can we provide an estimate of the dark current magnitude. However, a first approximation on the number of defects in each camera does indicate that with the smaller pixel size we are seeing more defective pixels per unit area than in regular cameras. As opposed to regular digital cameras, only simple procedures are taken to correct manufacture time defects; thus the defects identified in these cellphone cameras include both in-field and manufacture time defects, and will require a totally different analysis approach.

6. Conclusion

Defect developing is inevitable in any aging digital images. Our continuous analysis of spatial distribution and temporal growth of defects with an expanding number of defects (137 defects so far) has again shown no indication of material source related defects. Moreover, the higher number of defects observed in imagers that were exposed to high radiation environments indicates that cosmic ray radiation is the probable defect source. First approximation on defect growth rates based on a collection of APS and CCD imagers showed that the average growth rate of APS imagers is ~2.2 defects/year while for CCD imagers it is ~5.2 defects/year. While CCD developing defects at twice the rate of APS sensors, the suggestion is that CCD sensors may be more sensitive to cosmic ray radiation. With the development of an automated defect-tracing algorithm, we are able to detect the defect development date and estimate the defect growth rate of individual imagers by analyzing historical images from individual cameras, permitting this to eventually be expanded to many cameras. The accuracy of the detection algorithm is limited by false detections caused by scene complexity; however, by incorporating knowledge of the local region around the defect, we are able to correct some false defect detections. Our recent in-field tests on three imagers 2-5 years old with a total of 26 defects has shown that 96% of the defect dates were identified within 10 days of the visually identified dates. To expand our in-field defect analysis, we have extended our study to 10 cellphone cameras with a much smaller pixel size. Preliminary results showed that these cameras had ~117 defects prior to shipment by the manufacturer, because only simple techniques were used to map out manufacture time defects. Thus, defects identified in these cameras will include both manufacture-time and in-field defects and will require a new set of analysis tools.

7. References

[1] J. Leung, J. Dudas, G. H. Chapman, I. Koren, Z. Koren, "Quantitative Analysis of In-Field Defects in Image Sensor Arrays," *Proc. of the 2007 Intern. Symposium on Defect and Fault Tolerance in VLSI*, pp.526-534, Rome, Italy, Sept 2007.

[2] A. J.P. Theuwissen, "Influence of Terrestrial Cosmic Rays on the Reliability of CCD Image Sensors," IEDM 2005, San Francisco, CA, 2005.

[3] J. Leung, J. Dudas, G.H. Chapman, Z. Koren, and I. Koren, "Characterization of defect development During Digital Imager Lifetime," Proc. Electronic Imaging, Sensors, Cameras, and Systems for Industrial/Scientific Application IX, San Jose, Jan. 2008.

[4] J. Dudas, L.M. Wu, C. Jung, G.H. Chapman, Z. Koren, and I. Koren, "Identification of in-field defect development in digital image sensors," Proc. Electronic Imaging, Digital Photography III, v6502, 65020Y1-0Y12, San Jose, Jan. 2007.